Metallic transport in polyaniline

Kwanghee Lee[1,2]*, Shinuk Cho[1], Sung Heum Park[1], A. J. Heeger[2], Chan-Woo Lee[3] & Suck-Hyun Lee[3]*

Despite nearly three decades of materials development, the transport properties in the 'metallic state' of the so-called conducting polymers are still not typical of conventional metals[1–7]. The hallmark of metallic resistivity—a monotonic decrease in resistivity with temperature—has not been obtained at temperatures over the full range below room temperature; and a frequency dependent conductivity, $\sigma(\omega)$, typical of metals has also not been observed. In contrast, the low-temperature behaviour of 'metallic' polymers has, in all previous cases, exhibited an increase in resistivity as temperature is further decreased, as a result of disorder-induced localization of the charge carriers[1–4]. This disorder-induced localization also changes the infrared response such that $\sigma(\omega)$ deviates from the prediction of Drude theory[5–7]. Here we report classic metallic transport data obtained from truly metallic polymers. With polyaniline samples prepared using self-stabilized dispersion polymerization[8], we find that for samples having room-temperature conductivities in excess of 1,000 S cm^{-1}, the resistivity decreases monotonically as the temperature is lowered down to 5 K, and that the infrared spectra are characteristic of the conventional Drude model even at the lowest frequencies measured.

The dynamics of the single-particle excitations in the partially filled conduction band of traditional metals are governed by coherent diffusion processes[9]. Electrons drift ballistically with a mean free path much longer than the structural repeat length and make random collisions with defects and with phonons, resulting in finite resistivity. As shown by Landau, the low-energy excitations in metals can be treated as non-interacting quasiparticles and described by Fermi-liquid theory[10]. This theory rationalizes and fundamentally explains the success of the free-electron approximation (the Drude model) in describing the electronic properties of simple metals[11]. When disorder is introduced, with the magnitude of disorder potential comparable to the bandwidth, multiple scattering causes the electronic states near the Fermi energy (E_F) to become localized and thereby causes a transition from metal to insulator[12]. Strong disorder transforms the Fermi liquid into a 'Fermi glass'[13].

The disorder in metallic polymers arises from a combination of molecular-scale disorder[2,3] and structural inhomogeneities at mesoscopic length scales[4,6]. Even the most highly conducting polymers have been described as disordered metals near the metal–insulator transition[2,3]. They have a finite density of states at E_F, as verified by measurements of the Pauli spin susceptibility[14], the linear term in the temperature dependence of the thermoelectric power[15], and the linear term in the temperature dependent heat capacity[16]. Despite the finite density of states at E_F, the transport properties in the 'metallic state' as reported in the literature do not exhibit the traditional signatures of conventional metals. The d.c. conductivity (σ_{dc}) is thermally activated (phonon assisted), decreasing as the temperature is lowered[4,17–19], and $\sigma(\omega)$ is not consistent with Drude behaviour in the infrared[20–24]. In the best cases, resistivity as a function of temperature, $\rho(T)$, is nearly constant, with a weak minimum below

room temperature[2,3]. Thus, before this report, truly metallic transport has never been observed in conducting polymers.

Polyaniline (PANI) samples were prepared by self-stabilized dispersion polymerization (SSDP) as described in detail elsewhere[8]. In contrast to conventional homogeneous/dispersion polymerization using an aqueous medium containing aniline, acid and oxidant, this new polymerization was carried out in a heterogeneous biphasic (organic and aqueous) mixture without any stabilizers (Fig. 1). As the anilinium hydrochloride monomer is like a surfactant, with a polar hydrophilic part and an organic hydrophobic part, the monomers and growing polymer chains act as interfacial stabilizers, resulting in excellent dispersion of the organic phase inside the aqueous reaction medium. The organic phase tends to separate the aniline monomers and grown PANI chains from the reactive ends of the chain in the aqueous phase, thereby suppressing undesirable side reactions (such as *ortho*-coupling or Michael reductive additions). The reaction mixture was filtered, washed, deprotonated to the emeraldine base (EB) form, and then dried[8]. This synthesis produced high quality undoped PANI-EB samples with a low density of structural defects, as demonstrated in previous studies[8].

Free-standing films of emeraldine salt were prepared by doping PANI-EB with camphor sulphonic acid (CSA), giving PANI-CSA, and cast from solution in *meta*-cresol. Typical sample thicknesses were about 30 µm. Figure 2 shows the temperature dependence of ρ for a series of free-standing films of PANI-CSA. For comparison, we
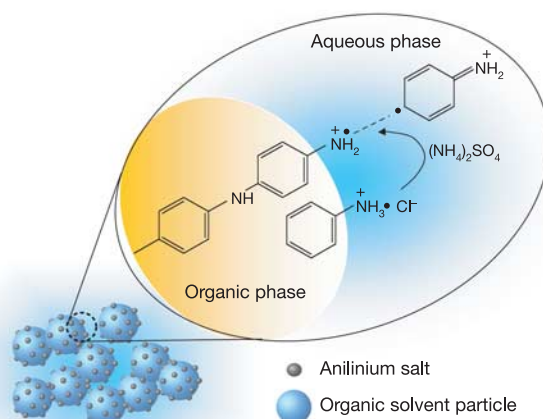

Figure 1 | Diagram of the self-stabilized dispersion polymerization of polyaniline. The polymerization is carried out in a heterogeneous biphasic (organic and aqueous) medium in order to prevent undesirable side reactions. The anilinium hydrochloride monomers locate on the surface of the organic solvent component and the radical is generated in the aqueous phase at the beginning of polymerization.

[1]Department of Physics, Pusan National University, Busan 609-735, Korea. [2]Center for Polymers and Organic Solids, University of California at Santa Barbara, Santa Barbara, California 93106-5090, USA. [3]Department of Molecular Science and Technology, Ajou University, Suwon 442-749, Korea.
*These authors contributed equally to this work.

also plot $\rho(T)$ for the PANI-CSA that was prepared by the standard polymerization method ($\sigma_{dc}(300\,K) \approx 270\,S\,cm^{-1}$, and resistivity ratio $\rho_r = \rho(5\,K)/\rho(300\,K) \approx 2.6$). Although the synthesis conditions are nominally identical for all samples, details of the film preparation and processing lead to differences in the sample quality, and thereby to changes in the electrical properties, as can be seen in Fig. 2. The SSDP samples exhibit significantly enhanced transport properties compared to those of conventional samples. As $\rho(300\,K)$ decreases, $\rho(T)$ remains progressively lower (σ_{dc} is higher) over the entire temperature range, the minimum in $\rho(T)$ shifts to lower temperatures, and the low temperature up-turn becomes less pronounced. For the highest conductivity samples, S1 and S2 (with respective $\sigma_{dc}(300\,K)$ values of $\sim 1{,}300\,S\,cm^{-1}$ and $1{,}100\,S\,cm^{-1}$), $\rho(T)$ exhibits a positive temperature dependence ($d\rho/dT > 0$) down to our low temperature measurement limit of 5 K with $\rho_r \approx 0.4$ for S1 (10 K for S2), as shown in Fig. 2 inset. Measurements of $\rho(T)$ below 5 K are under way for the highest conductivity samples.

The metallic nature of SSDP samples was confirmed by measurements of the reflectance, $R(\omega)$, at room temperature (Fig. 3a). Reflectance measurements were made of samples taken from all the synthesis batches. The data obtained from S1 and S2 (Fig. 2) were almost indistinguishable; the data shown in Fig. 3a were obtained from S2. In the far-infrared, $R(\omega) > 0.8$; $R(\omega)$ drops throughout the mid-infrared to a minimum at 1.4 eV, indicative of the free-carrier plasma resonance characteristic of a metal. Above the 1.4 eV minimum, $R(\omega)$ shows weak structure around 2.7 eV associated with the interband transition well known in doped PANI (and associated with the characteristic green colour). As shown in the inset of Fig. 3a, the Hagen-Rubens (H-R) approximation provides an excellent fit to $R(\omega)$ in the far-infrared.

The weak structure in the mid-infrared ($1{,}000$–$1{,}500\,cm^{-1}$) arises from the infrared-active vibration (IRAV) modes characteristics of conducting polymers. Note, however, that the IRAV modes of these highest conductivity sampl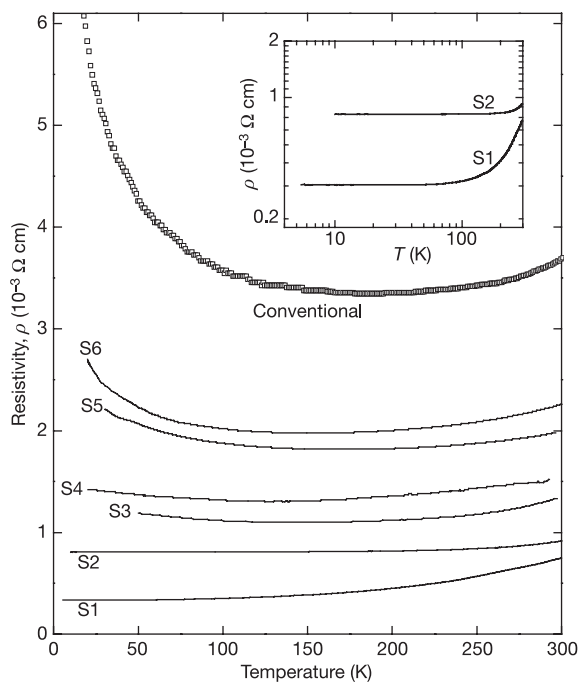es are particularly weak compared to those reported earlier for 'metallic' polyaniline[20]. The IRAV modes in conducting polymers are characteristic of localized states, either self-localized states associated with solitons and polarons or localized states induced by disorder. When charges occupy such localized states, they move in response to the electric field of the infrared radiation and indirectly drive the amplitude modes, causing the Raman-active modes to become infrared-active. In the metallic regime, however, where the Fermi velocity is much greater than sound velocity, we do not expect to observe resonant IRAV modes. Thus, the reduced oscillator strength of the IRAV modes is consistent with the $\rho(T)$ data and implies that the metallic PANI-CSA characterized in Figs 2 and 3 is well beyond the insulator-to-metal transition.

Although the spectral features in $R(\omega)$ are similar to those of conventional PANI-CSA, the higher quality of the present samples is
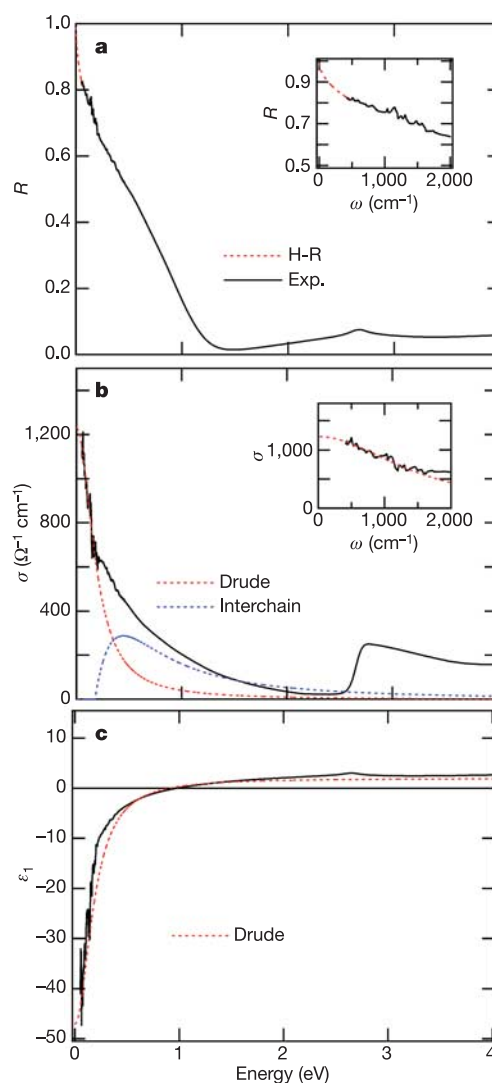

Figure 3 | Optical spectra of high-conductivity PANI-CSA. a, Reflectance spectra, $R(\omega)$ (solid line shown as 'Exp.'). The Hagen-Rubens approximation (H-R, red dotted line) provides an excellent fit to $R(\omega)$ in the far-infrared. The inset shows $R(\omega)$ below $2{,}000\,cm^{-1}$ with an expanded scale. **b,** Frequency dependent conductivity, $\sigma(\omega)$ (solid line), as obtained from Kramers-Kronig analysis of $R(\omega)$. The red dotted line represents the theoretical fit by the Drude model, $\sigma_D(\omega) = (\omega_p^2 \tau/4\pi)(1 + \omega^2 \tau^2)^{-1}$, with $\omega_p = 10{,}500\,cm^{-1}$ and $\tau = 2.2 \times 10^{-14}\,s$, whereas the blue dotted line corresponds to the interchain contribution to $\sigma(\omega)$. **c,** The real part of the dielectric function, $\varepsilon_1(\omega)$ (solid curve). The red dotted line represents the theoretical fit by the Drude model, $\varepsilon_{1D}(\omega) = \varepsilon_\infty - \omega_p^2 \tau^2 (1 + \omega^2 \tau^2)^{-1}$, using the same parameters as in Fig. 3b.

Figure 2 | Temperature dependence of resistivity, $\rho(T)$. Data from a conventional PANI-CSA film are shown for comparison. The SSDP PANI-CSA samples exhibit significantly enhanced conductivities compared with that obtained from the conventional sample. For more highly conducting samples (S5 → S1), the resistivity minimum weakens and shifts down to lower temperature and eventually disappears in the S1 and S2 samples (as shown more clearly in the inset).

evident from the optical conductivity, $\sigma(\omega)$, and the real part of the dielectric function, $\varepsilon_1(\omega)$, as obtained through the Kramers-Kronig (K-K) analysis. Figure 3b shows $\sigma(\omega)$ for sample S2. In contrast with the results obtained from conventional conducting polymers[20–24], in which $\sigma(\omega)$ decreases below $\omega = 2{,}500\,\text{cm}^{-1}$, the PANI-CSA data in Fig. 3b follow the typical Drude frequency dependence at low frequencies (below $2{,}000\,\text{cm}^{-1}$) and approaches the measured $\sigma_{\text{dc}}(300\,\text{K})$. The excellent fit to $\sigma(\omega)$ of the classical Drude model, $\sigma_D(\omega) = (\omega_p^2 \tau/4\pi)(1 + \omega^2\tau^2)^{-1}$, with the plasma frequency $\omega_p = 10{,}500\,\text{cm}^{-1}$ ($\sim$1.3 eV) and relaxation time $\tau = 2.2 \times 10^{-14}\,\text{s}$ ($1/\tau = 1{,}500\,\text{cm}^{-1} = 0.19\,\text{eV}$), is shown in Fig. 3b inset. For $\omega > 2{,}000\,\text{cm}^{-1}$, the interchain contribution starts to dominate $\sigma(\omega)$, consistent with previous studies[25].

The $\varepsilon_1(\omega)$ spectrum is also consistent with the Drude model and true metallic behaviour. The fit to $\varepsilon_1(\omega)$ of the Drude model, $\varepsilon_{1D}(\omega) = \varepsilon_\infty - [\omega_p^2\tau^2(1 + \omega^2\tau^2)^{-1}]$, with the same values of ω_p and τ as in $\sigma_D(\omega)$ and with the high frequency dielectric constant $\varepsilon_\infty \approx 2$, shows again good agreement with the data (Fig. 3c). In the data obtained from earlier reflectance studies of conducting polymers[20], ε_1 crosses zero and becomes negative at the screened plasma frequency given by $\Omega_p = \omega_p/(\varepsilon_\infty)^{1/2}$, as expected for a typical metal. However, in contrast to simple Drude behaviour, $\varepsilon_1(\omega)$ crosses zero again to positive values around $\omega \approx 2{,}500\,\text{cm}^{-1}$ and remains positive down to $\sim 20\,\text{cm}^{-1}$. The $\varepsilon_1(\omega)$ data for PANI-CSA reported here, however, cross zero at $\omega = 7{,}800\,\text{cm}^{-1}$ ($=0.97\,\text{eV}$) and remain negative at all frequencies below $7{,}800\,\text{cm}^{-1}$, again consistent with the classic Drude model.

The parameters obtained from the Drude fit are reasonable and consistent with other experimental results. The plasma frequency $\omega_p \approx 1.3\,\text{eV}$ is in good agreement with the $R(\omega)$ minimum around 1.4 eV, and yields $\Omega_p \approx 1\,\text{eV}$ with $\varepsilon_\infty \approx 2$, which is exactly consistent with the zero-crossing frequency in $\varepsilon_1(\omega)$. Using these parameters,
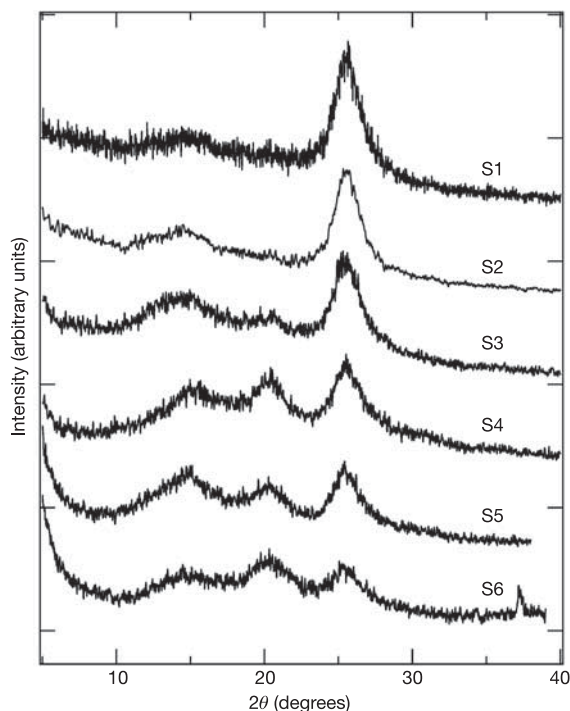
we estimate the d.c. conductivity to be $\sigma_D(\omega = 0) = \omega_p^2\tau/4\pi \approx 1{,}200\,\text{S\,cm}^{-1}$, in good agreement with the measured $\sigma_{\text{dc}}(300\,\text{K}) \approx 1{,}100\,\text{S\,cm}^{-1}$. Moreover, from the relation $\omega_p = (4\pi ne^2/m^\star)^{1/2}$ where n is the charge carrier density and $m^\star$ is the effective mass, we obtain $n = 2.5 \times 10^{21}\,\text{cm}^{-3}$ with the reasonable assumption of $m^\star \approx 2m_e$ (m_e, free electron mass) for this class of materials[20,21]. This result is consistent with that obtained from Hall measurements on this sample; the Hall effect data give $n_{\text{Hall}} = 2.1 \times 10^{21}\,\text{cm}^{-3}$. In the previous studies on conventional conducting polymers[20,21], the proper description of the charge dynamics was achieved only after 'modifying' the Drude model in the context of weak localization. However, the excellent agreement established here demonstrates that high conductivity PANI-CSA can be successfully described by the simple Drude model without incorporating any contributions from disorder-induced localization theory.

We attribute the present results to the improved molecular structure of PANI-CSA prepared by SSDP. X-ray diffraction (XRD) patterns of films (taken in the reflection geometry) are shown in Fig. 4. For the lowest conductivity sample (S6), the diffraction pattern is almost identical with that reported earlier for PANI-CSA, consisting of three sharp peaks superimposed on a broad scattering background indicative of crystalline regions dispersed in an amorphous medium[26,27]. However, for the more metallic samples (S5 → S1) the broad background decreases, and the relative intensity of the three peaks (at 15°, 20° and 25°) changes: the peaks at 15° and 20° decrease and become nearly indistinguishable from the background, whereas the peak at 25° increases and sharpens. As a consequence, for the highest conductivity samples with $d\rho(T)/dT > 0$, the diffraction pattern is dominated by the peak at 25°. The d-spacing ($\sim$3.5 Å) associated with the diffraction peak at 25° corresponds to the face-to-face interchain stacking distance between phenyl rings. Thus, the increase in the intensity of the 25° peak along with the decrease in background intensity implies improved π–π interchain stacking. This suggests a more planar chain conformation with reduced torsion angles between the phenyl ring and the plane of the backbone, resulting in elongation of the effective conjugation length. These initial structural data are qualitatively consistent with improved carrier transport and a longer mean free path.

The achievement of metallic samples well on the metallic side of the insulator–metal transition for PANI-CSA implies that the promise of high performance semiconducting and metallic polymers could be realized by improving the material quality of known polymer systems. The utilization of such high performance semiconducting and metallic polymers in 'plastic electronics' would significantly extend the range of possible applications.

METHODS

Polyaniline samples were prepared at the Department of Molecular Science and Technology, Ajou University. All measurements ($\rho(T)$ versus T, optical reflectance, and XRD) were carried out in the Physics Department at Pusan National University. For the $\rho(T)$ versus T measurements, both the standard four-probe method and the Van der Pauw method were used in a closed cycle cryogenic system. A sapphire (Al_2O_3) plate was used to thermally anchor the samples to the Cu cold fingers; the samples were mounted on the sapphire plate using a GE-varnish adhesive. Gold wires in a four-probe configuration were connected parallel to the sample surface. Electrical contacts were made with conducting graphite adhesive. The current was applied using a Keithley 237 current source, while the voltage drop was measured using a Keithley 181 nanovoltmeter.

Each of the data sets in Fig. 2 was obtained from measurements of three independent samples from material from a single synthesis. Two samples were measured using the four-probe method, while a third sample was measured using the Van der Pauw method. The data from all three measurements were consistent and in quantitative agreement within experimental error. The highest conductivity data (S1) were obtained from three different samples taken from material from a single synthesis run. Materials with $\sigma_{\text{dc}}(300\,\text{K}) \approx 1{,}100\,\text{S\,cm}^{-1}$ (or less) were obtained from several independent synthesis runs.

Optical reflectance spectra were measured between 0.04 and 6.2 eV using two different spectrometers. Infrared reflectance in the range 0.04–0.5 eV was measured with a Mattson 5000 Fourier transform interferometer (FTIR),

Figure 4 | X-ray diffraction patterns of the SSDP PANI-CSA samples. The low conductivity sample (S6) is almost identical with that of the conventional PANI. For the more metallic samples (S5 → S1), the broad background from the amorphous phase disappears and the crystalline peaks (at 15°, 20° and 25°) change gradually. For the best metallic samples (S1 and S2), the peak at 25° dominates (the background and the peaks at 15° and 20° have nearly disappeared).

while a Varian Cary 5E spectrophotometer covered the spectral range 0.4–6.2 eV. A gold mirror was used as the reference in the infrared range, and an aluminium mirror was used in the visible-ultraviolet range.

XRD experiments were performed using a conventional X-ray scanning diffractometer (Rigaku X-ray). The X-ray radiation source was Cu-Kα radiation ($\lambda = 1.5418$ Å), and the scattered radiation diffractograms were collected over the range $2\theta \approx 5$–40° in a reflection geometry.

1. Heeger, A. J. Nobel Lecture: Semiconducting and metallic polymers: The fourth generation of polymeric materials. *Rev. Mod. Phys.* **73,** 681–700 (2001).
2. Menon, R., Yoon, C. O., Moses, D. & Heeger, A. J. in *Handbook of Conducting Polymers* 2nd edn (eds Skotheim, T. A., Elsenbaumer, R. L. & Reynolds, J. R.) 27–84 (Marcel Dekker, New York, 1998).
3. Heeger, A. J. The critical regime of the metal-insulator transition in conducting polymers: experimental studies. *Phys. Scr.* **T102,** 30–35 (2002).
4. Kaiser, A. B. Systematic conductivity behaviour in conducting polymers: effects of heterogeneous disorder. *Adv. Mater.* **13,** 927–941 (2001).
5. Kiebooms, R., Menon, R. & Lee, K. in *Handbook of Advanced Electronic and Photonic Materials and Devices* Vol. 8 (ed. Nalwa, H. S.) 1–102 (Academic, San Diego, 2001).
6. Kohlman, R. S., Joo, J. & Epstein, A. J. in *Physical Properties of Polymers Handbook* (ed. Mark, J. E.) 453–478 (AIP, New York, 1996).
7. Lee, K. in *Encyclopedia of Nanoscience and Nanotechnology* Vol. 5 (ed. Nalwa, H. S.) 537–549 (American Scientific Publishers, San Diego, 2004).
8. Lee, S.-H., Lee, D.-H., Lee, K. & Lee, C.-W. High-performance polyaniline prepared via polymerization in a self-stabilized dispersion. *Adv. Funct. Mater.* **15,** 1495–1500 (2005).
9. Ashcroft, N. W. & Mermin, N. D. *Solid State Physics* (Saunders College, New York, 1976).
10. Landau, L. D. The theory of a Fermi liquid. *Sov. Phys. JETP* **3,** 920–925 (1957).
11. Pines, I. D. & Nozieres, P. *The Theory of Quantum Liquids* (Benjamin, Menlo Park, 1966).
12. Mott, N. F. *Metal-insulator Transitions* (Taylor & Francis, London, 1990).
13. Anderson, P. W. The Fermi glass: theory and experiment. *Comments Solid State Phys.* **2,** 193–198 (1970).
14. Fite, C., Cao, Y. & Heeger, A. J. Magnetic susceptibility of one-dimensional metallic chains in solution. *Solid State Commun.* **73,** 607–609 (1990).
15. Park, Y. W., Choi, E. S. & Suh, D. S. Metallic temperature dependence of resistivity in perchlorate doped polyacetylene. *Synth. Met.* **96,** 81–86 (1998).
16. Moses, D., Denenstein, A., Pron, A., Heeger, A. J. & MacDiarmid, A. G. Specific heats of pure and doped polyacetylene. *Solid State Commun.* **36,** 219–224 (1980).
17. Reghu, M., Cao, Y., Moses, D. & Heeger, A. J. Counterion-induced processibility of polyaniline: transport at the metal-insulator boundary. *Phys. Rev. B* **47,** 1758–1764 (1993).
18. Yoon, C. O., Reghu, M., Moses, D. & Heeger, A. J. Transport near the metal-insulator transition: polypyrrole doped with PF$_6$. *Phys. Rev. B* **49,** 10851–10863 (1994).
19. Wang, Z. H., Scherr, E. M., MacDiarmid, A. G. & Epstein, A. J. Transport and EPR studies of polyaniline: a quasi one-dimensional conductor with three dimensional "metallic" states. *Phys. Rev. B* **45,** 4190–4202 (1992).
20. Lee, K., Heeger, A. J. & Cao, Y. Reflectance of polyaniline protonated with camphor sulfonic acid: disordered metal on the metal-insulator boundary. *Phys. Rev. B* **48,** 14884–14891 (1993).
21. Lee, K. *et al.* Nature of the metallic state in conducting polypyrrole. *Adv. Mater.* **10,** 456–459 (1998).
22. Kohlman, R. S. *et al.* Limit for metallic conductivity in conducting polymers. *Phys. Rev. Lett.* **78,** 3915–3918 (1995).
23. Chapman, B. *et al.* Low-energy conductivity of PF$_6$-doped polypyrrole. *Phys. Rev. B* **60,** 13479–13483 (1999).
24. Tzamalis, G., Zaidi, N. A., Homes, C. C. & Monkman, A. P. Doping-dependent studies of the Anderson-Mott localization in polyaniline at the metal-insulator boundary. *Phys. Rev. B* **66,** 085202 (2002).
25. Lee, K. & Heeger, A. J. Optical investigation of intra and interchain charge dynamics in conducting polymers. *Synth. Met.* **128,** 279–282 (2002).
26. MacDiarmid, A. G. & Epstein, A. J. Secondary doping in polyaniline. *Synth. Met.* **69,** 85–92 (1995).
27. Yan, H., Ohta, T. & Toshima, N. Stretched polyaniline films doped by (±)-10-camphorsulfonic acid: anisotropy and improvement of thermoelectric properties. *Macromol. Mater. Eng.* **286,** 139–142 (2001).